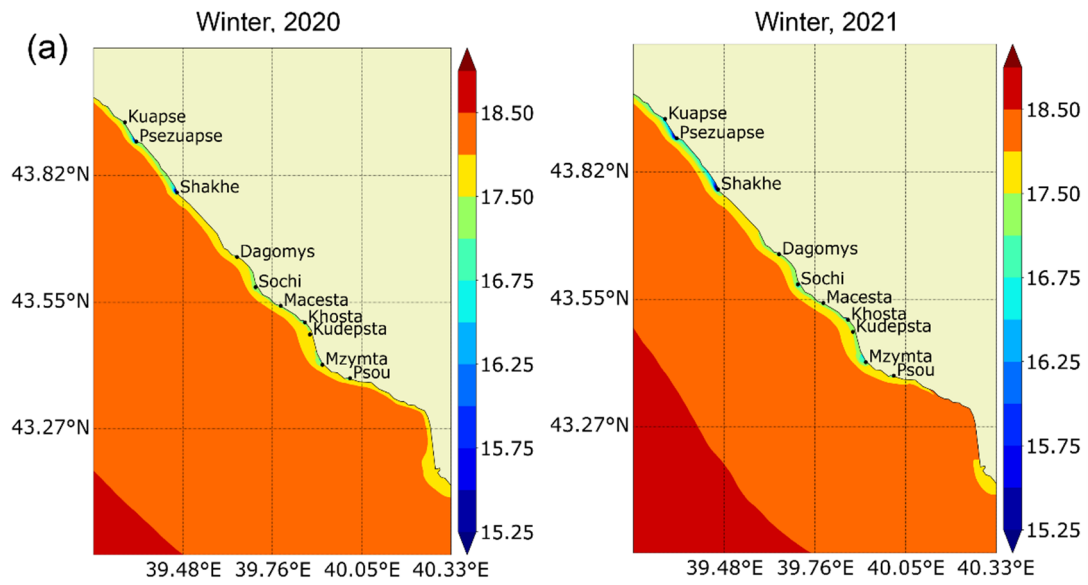


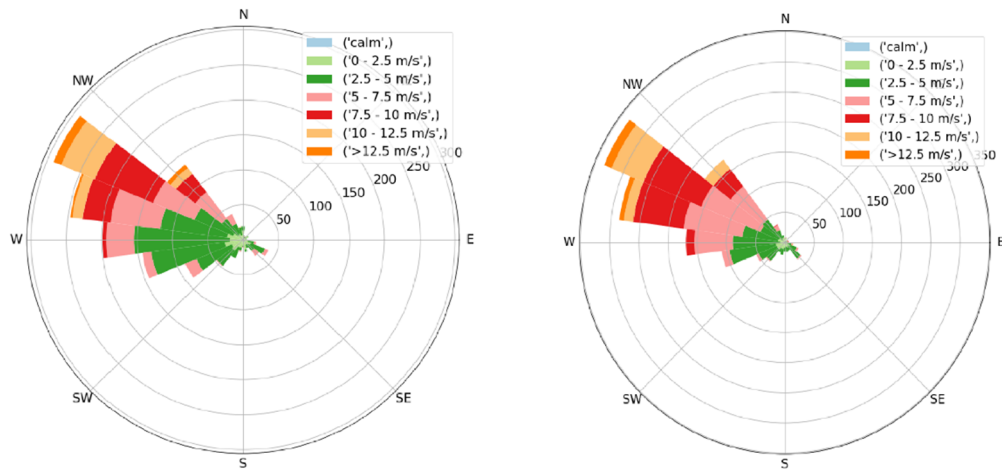
Supplementary Materials—1. Additional tables and figures

Table S1. Periods (month, date), duration (day), maximum discharge peak (m³/s), and total discharge (km³) of spring/spring–summer snowmelt freshets and flooding events in 2020–2021 for the Mzymta and Sochi rivers.

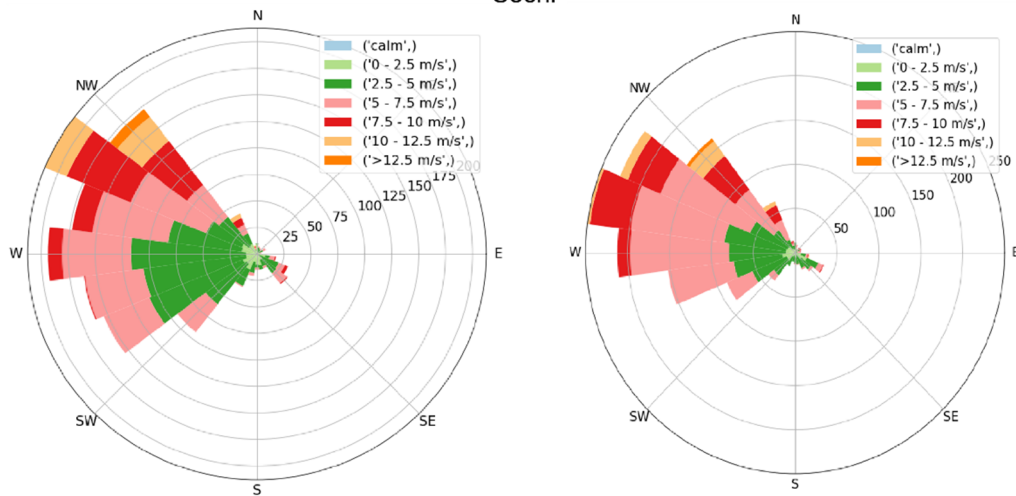
River/year	Periods	Duration	Maximum discharge peak	Total discharge
Flooding events				
Mzymta 2020	January–February	29.01–14.02	17	228.5
	December	21.12–24.12	4	17.4
	Spring/spring–summer snowmelt freshet			0.109
	February–July	24.02–31.07	159	198.2
Flooding events				
Sochi 2020	January–February	29.01–10.02	13	153.7
	April	16.04–19.04	4	41.6
	May	23.05–28.05	6	51.3
	November	01.11–03.11	3	10.5
	Spring/spring–summer snowmelt freshet			0.002
	February–March	24.02–22.03	28	73.1
Flooding events				
Mzymta 2021	January	10.01–21.01	12	137.9
	February	05.02–18.02	14	79.5
	February–March	28.02–01.03	2	30.6
	August	13.08–14.08	2	62.2
	September	03.09–04.09	2	71.9
	September	17.09	1	33
	September–October	24.09–02.10	9	68.9
	October	04.10–08.10	5	89.9
	November	24.11	1	78
	November–December	29.11–07.12	9	192
	December	09.12–10.12	2	49.9
	December	18.12	1	53.2
	December	20.12–22.12	3	82.5
	Spring/spring–summer snowmelt freshet			0.015
	16.03–05.08	16.03–05.08	143	332
Flooding events				
Sochi 2021	January	11.01–21.01	11	76.2
	February	5.02–17.02	13	36.8
	March	16.03–21.03	6	42.5
	March	23.03–28.03	6	121
	May	09.05–11.05	3	35.5
	June	02.06–10.06	9	107
	July	05.07–08.07	4	78.5
	July	23.07–24.07	2	30.5
	August	13.08	1	51.4
	September	3.09	1	27.7
	September	25.09–26.09	2	55.3
	October	04.10–06.10	3	44.4
	November	20.11–21.11	2	61.4
	November	24.11–25.11	2	68.7
	November	29.11–03.12	5	49.4
	December	17.12–22.12	6	38.5
	Spring/spring–summer snowmelt flood			0.013
	April–May	01.04–05.05	35	91.6

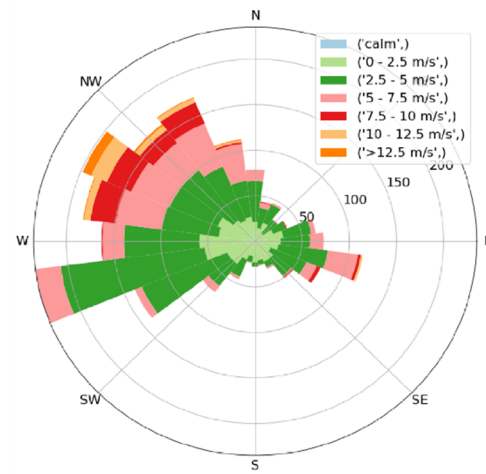
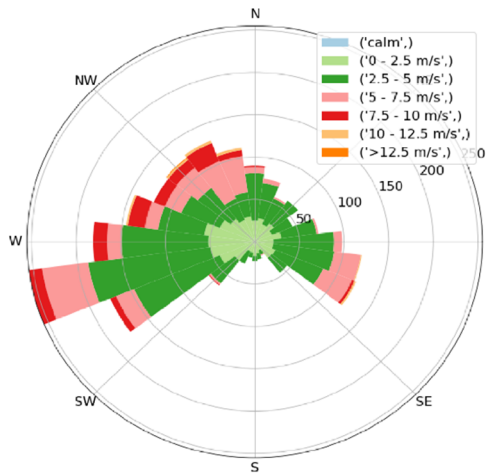
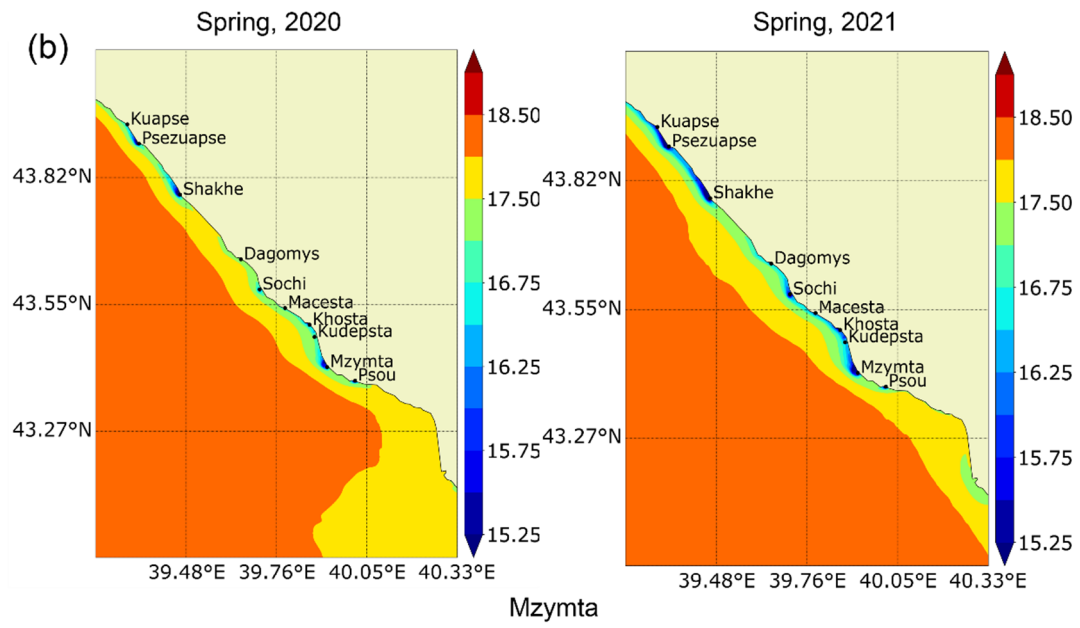


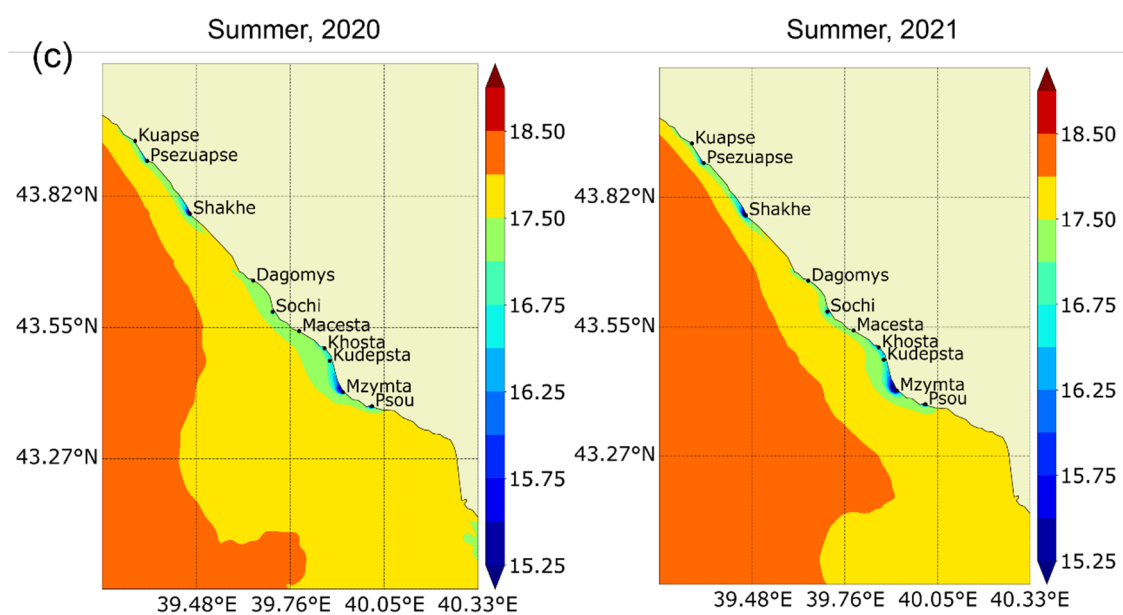
Mzymta



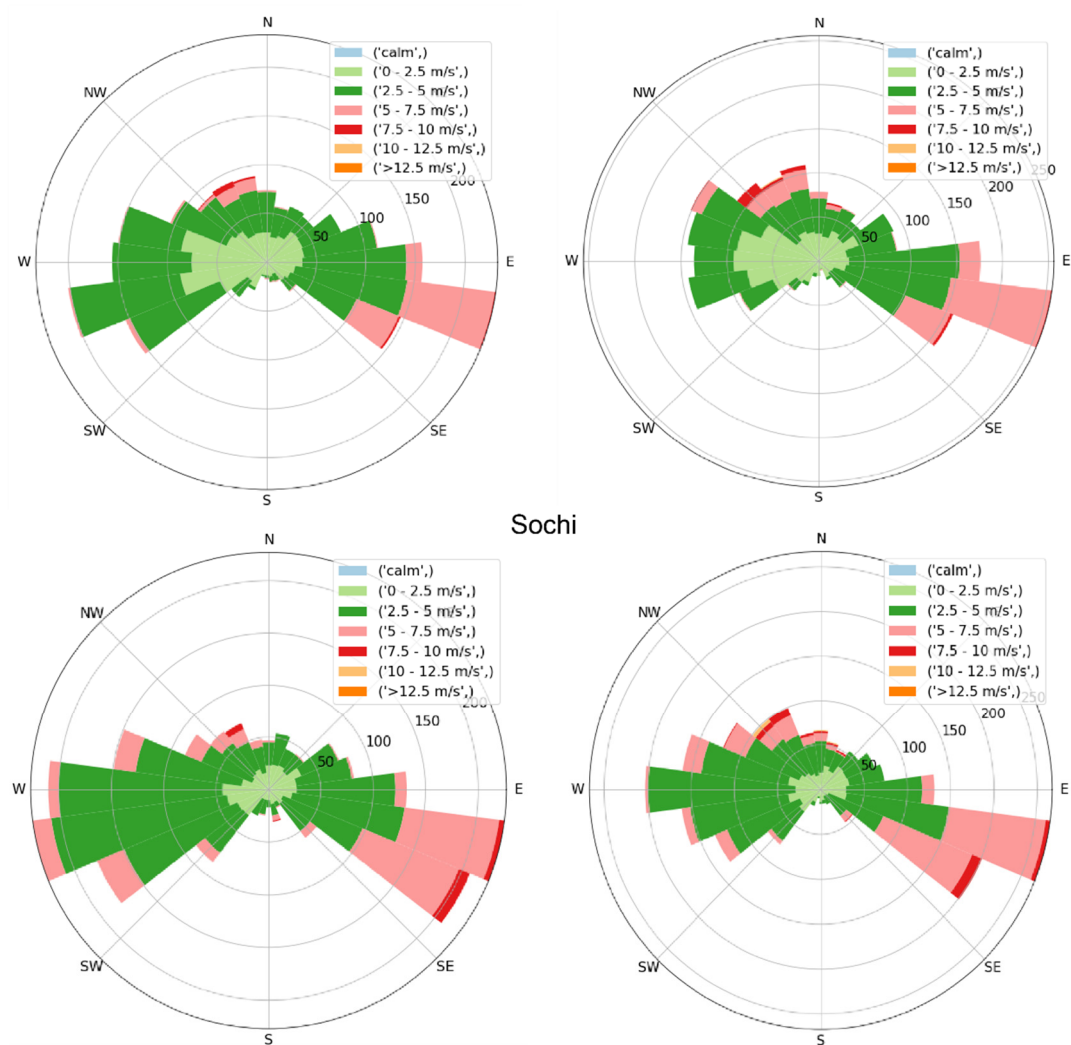
Sochi







Mzymta



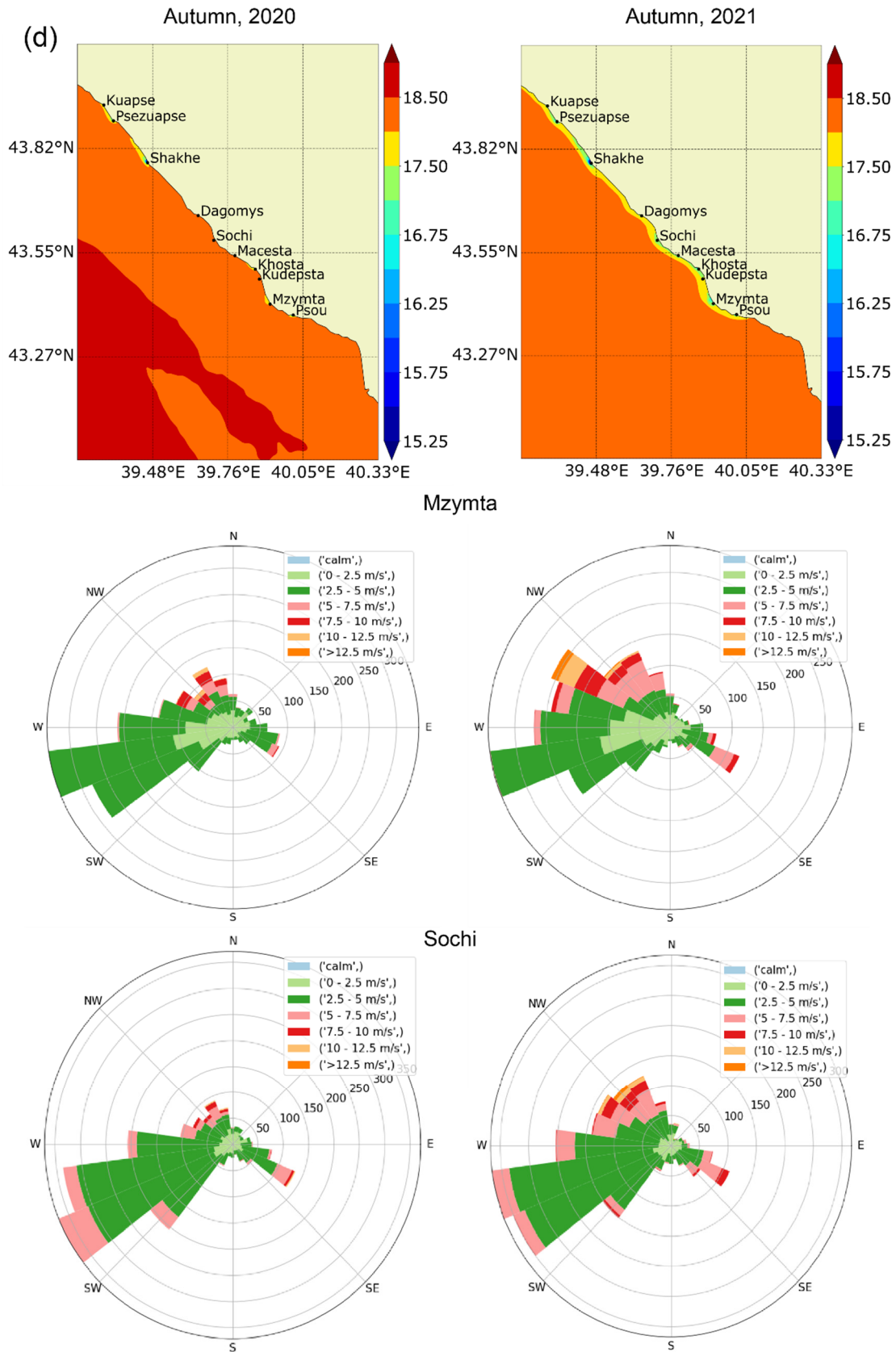
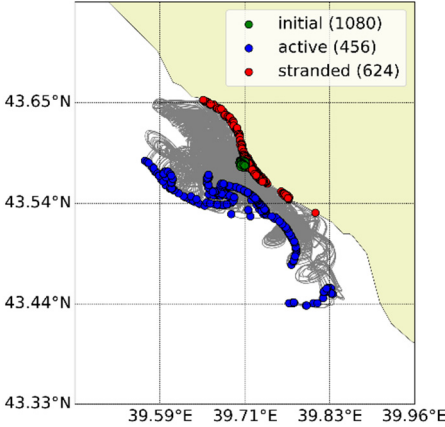
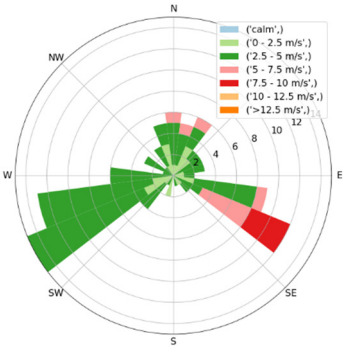


Figure S1. Seasonal fields (a–d) of surface salinity, according to the INMOM model analysis results, in the northeastern part of the Black Sea, and wind roses, according to the WRF model, at the mouths of the Mzymta and Sochi rivers for the low-discharge year of 2020 (left) and the high-discharge year of 2021 (right). The scale of the surface salinity fields is presented in psu. Wind speed is presented in m/s.

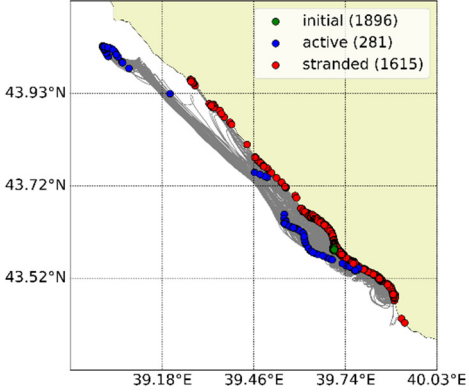
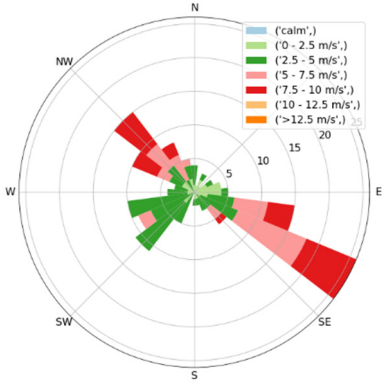
Table S2. Periods of flooding events, wind roses at river mouths, and distribution of Lagrangian particles (river water) during 2020–2021 for the Mzymta and Sochi rivers.

River/year	Periods	Wind roses	Distribution of Lagrangian particles
Mzymta 2020	29.01–14.02		
	21.12–24.12		
Sochi 2020	29.01–10.02		

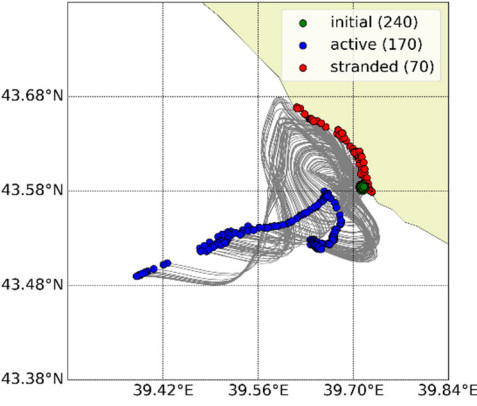
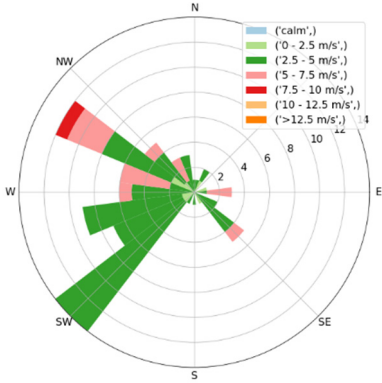
16.04–19.04



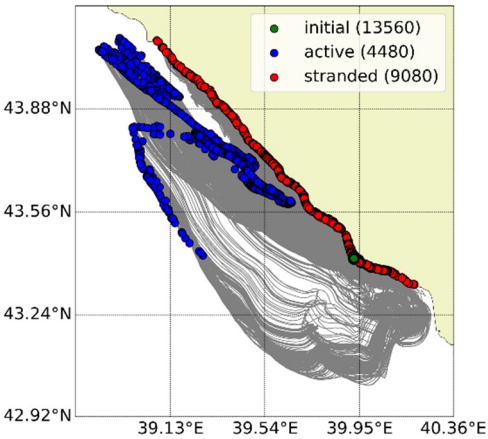
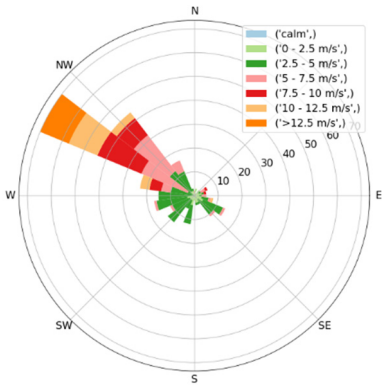
23.05–28.05



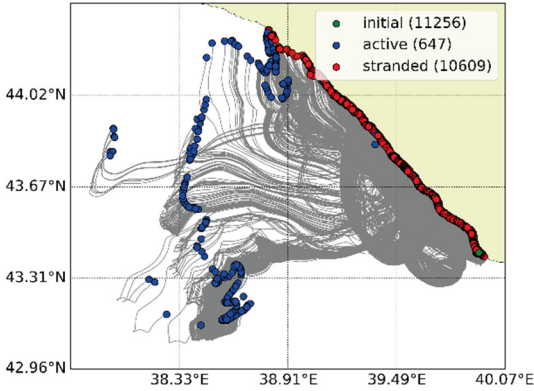
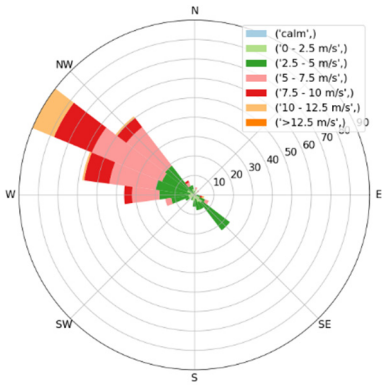
01.11–03.11



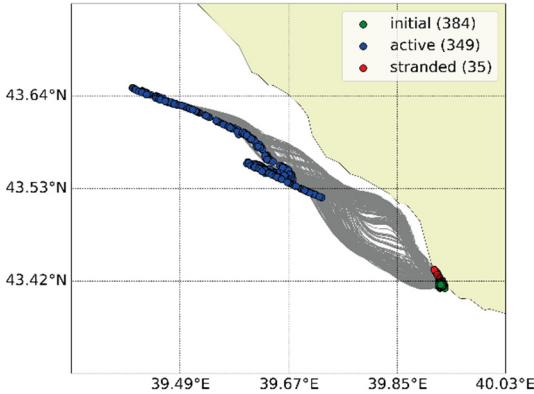
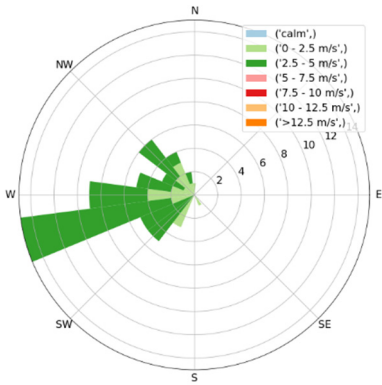
10.01–21.01



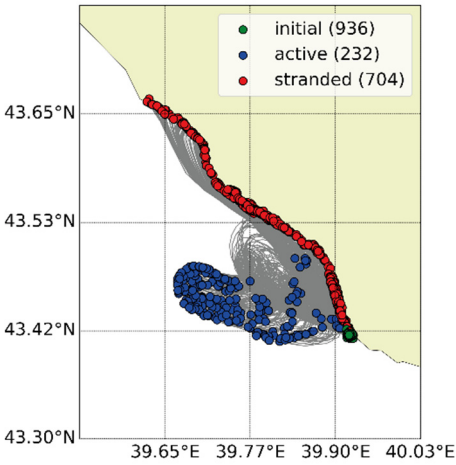
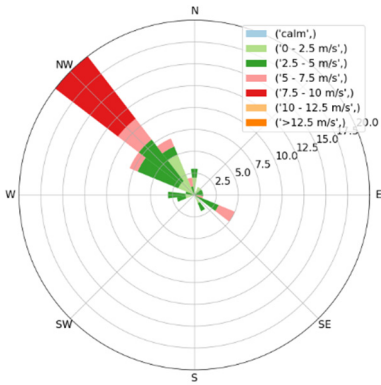
Mzymta 2021 05.02–18.02



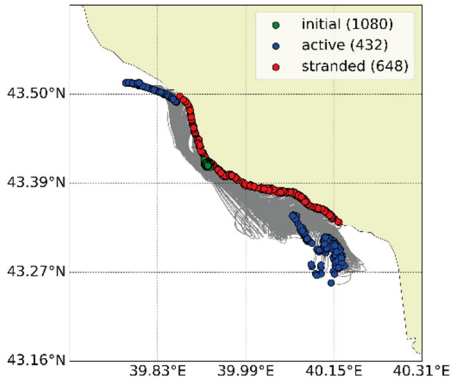
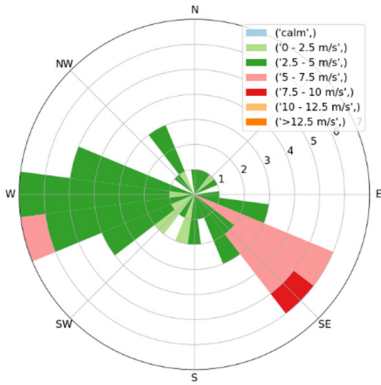
28.02–01.03



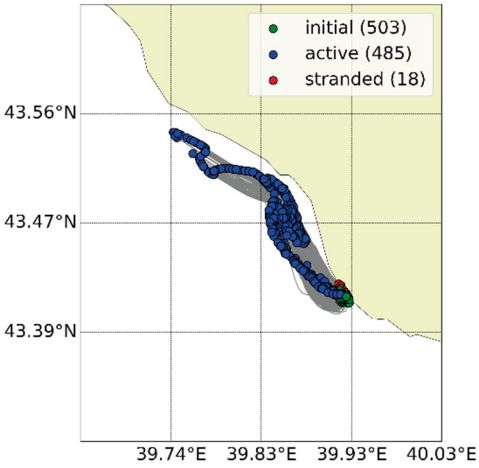
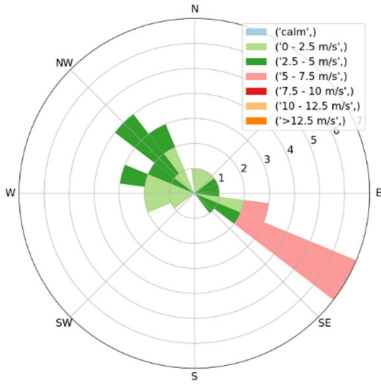
13.08–14.08



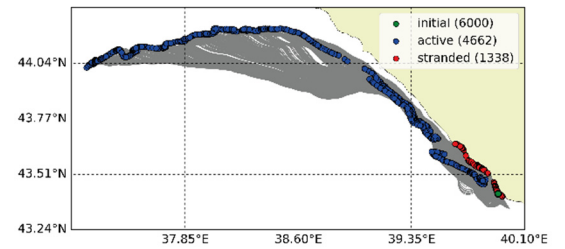
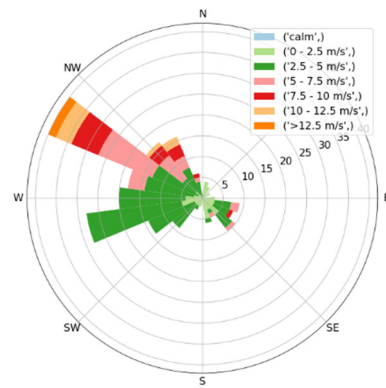
03.09–04.09



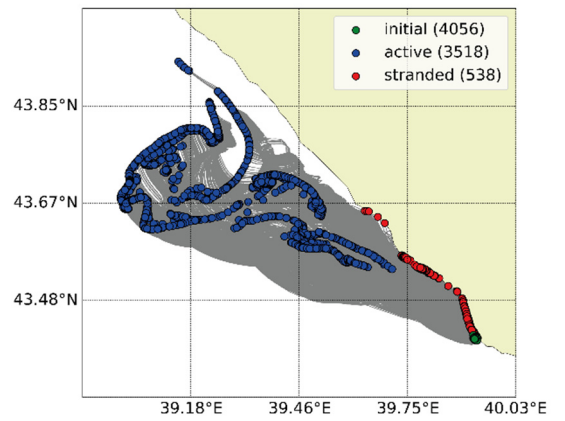
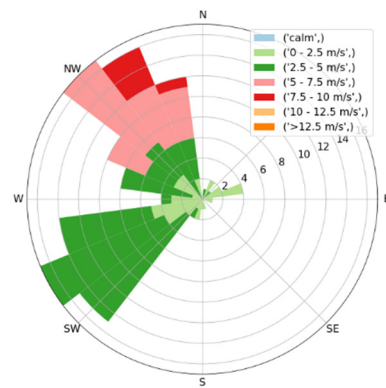
17.09



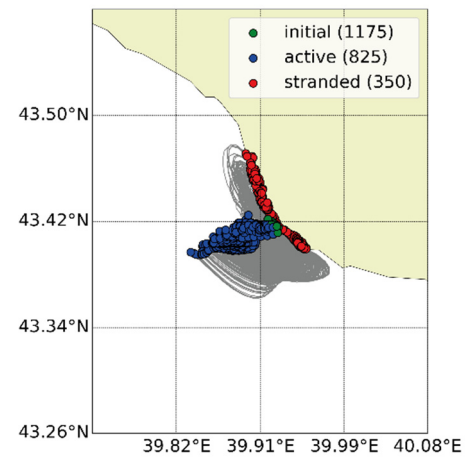
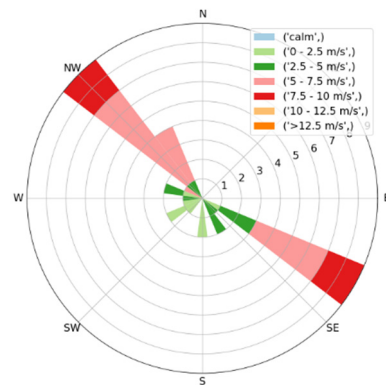
24.09–02.10



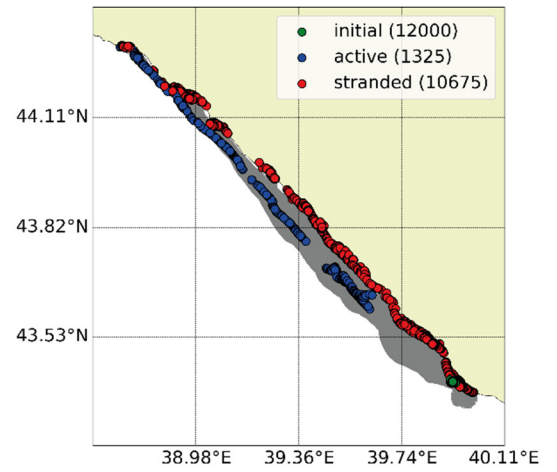
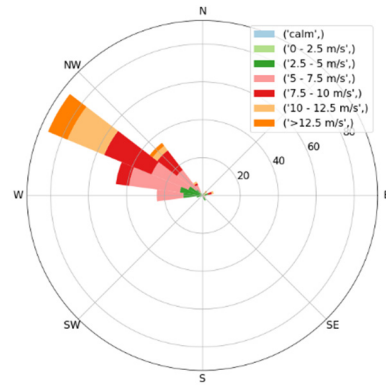
04.10–08.10



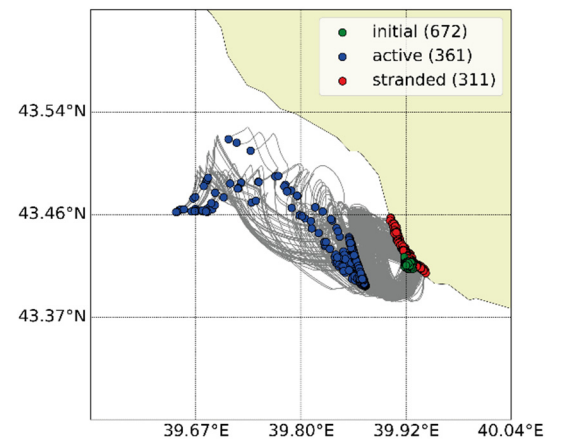
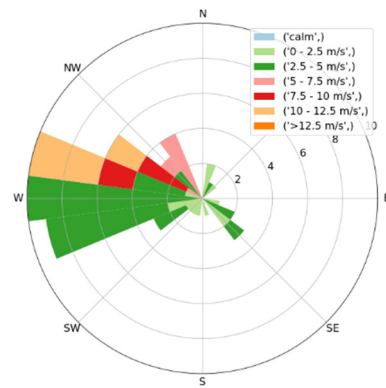
24.11



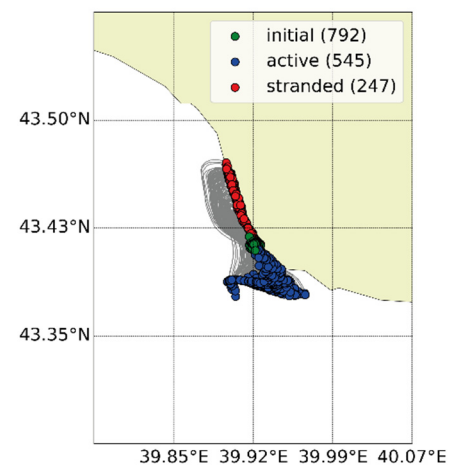
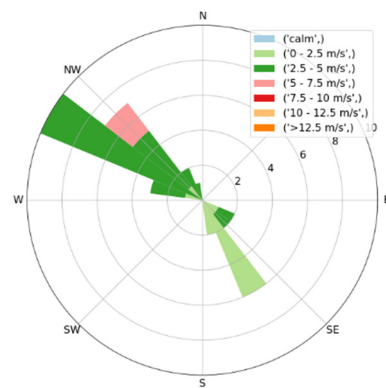
29.11–07.12



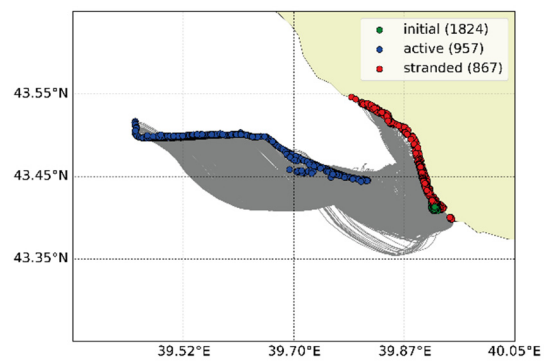
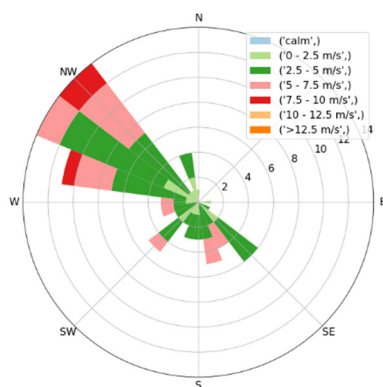
09.12–10.12



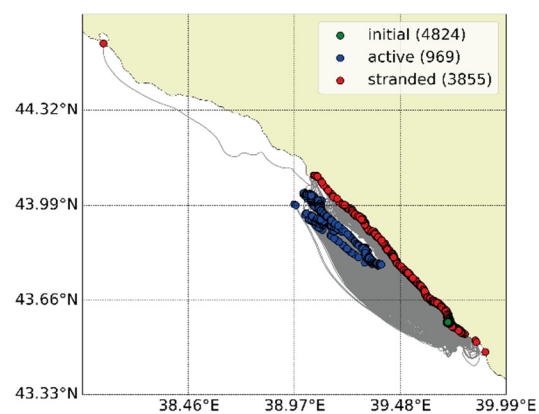
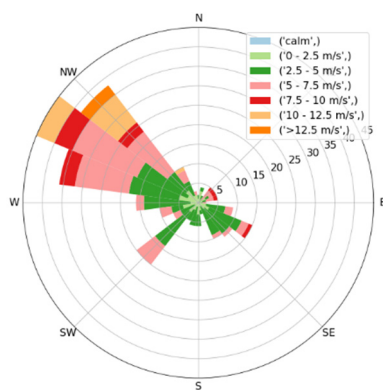
18.12



20.12–22.12

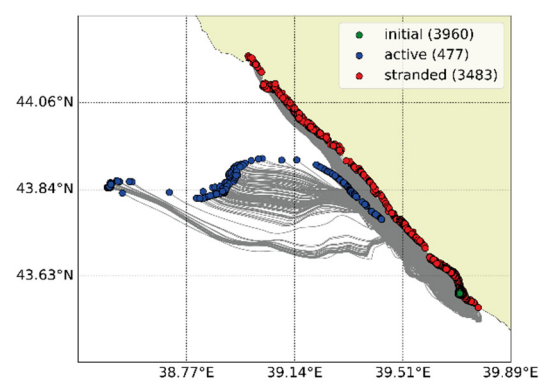
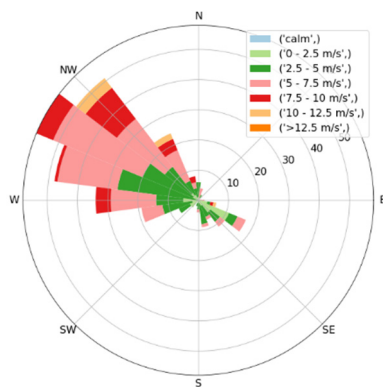


11.01–21.01

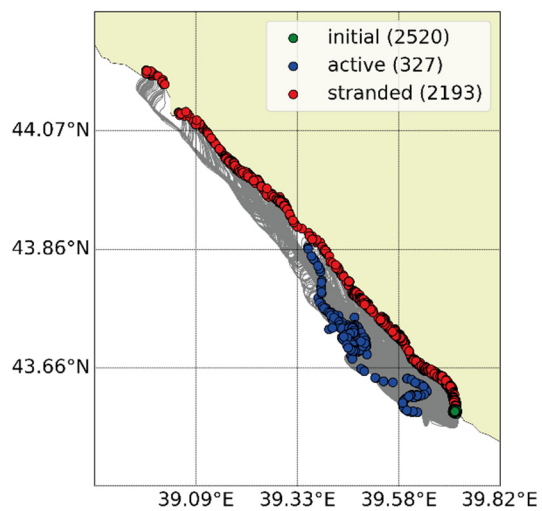
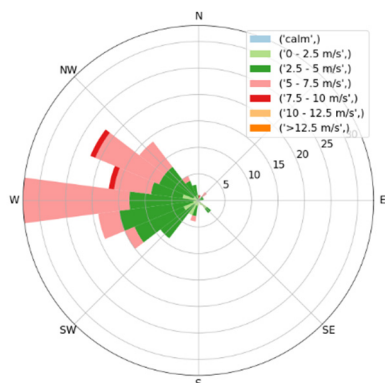


Sochi 2021

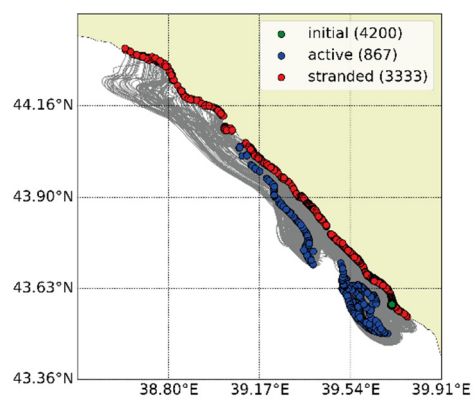
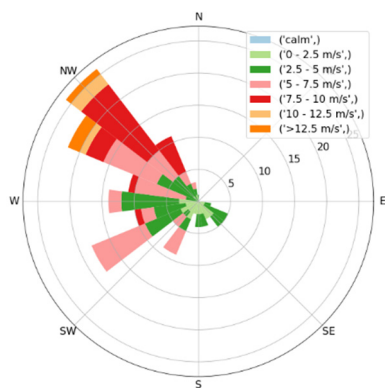
5.02–17.02



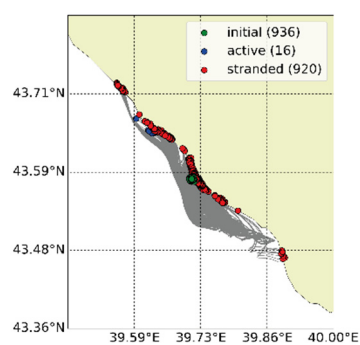
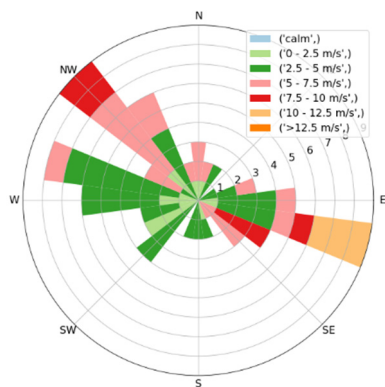
16.03–21.03



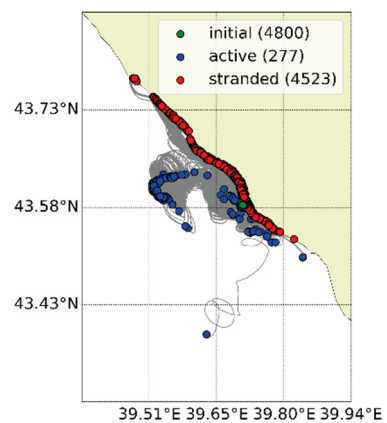
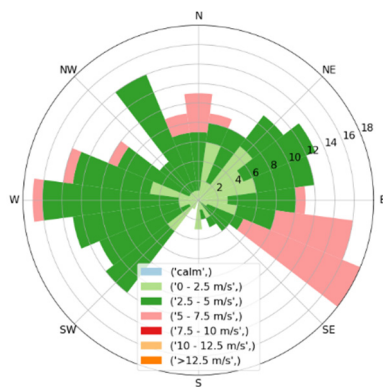
23.03–28.03



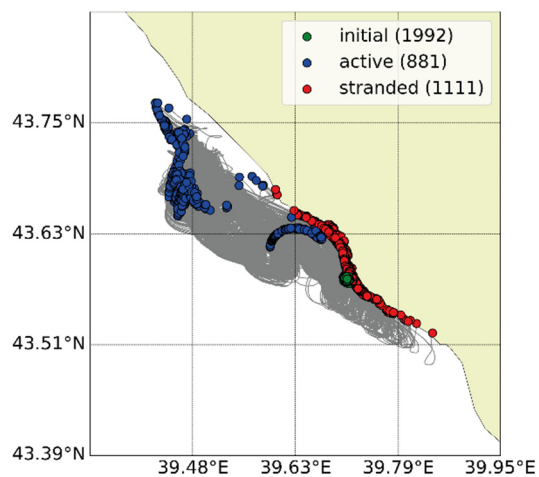
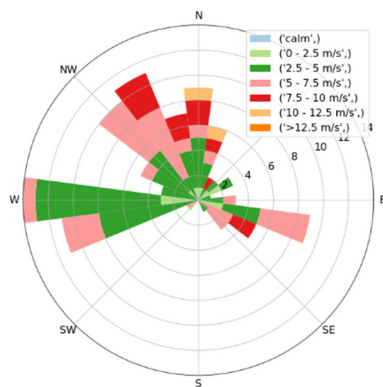
09.05–11.05



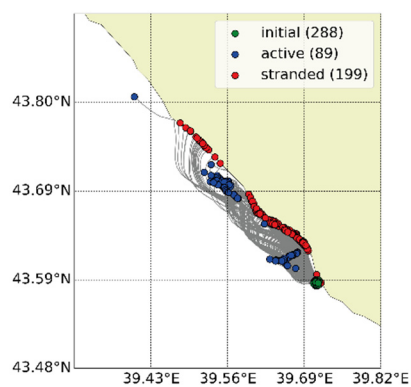
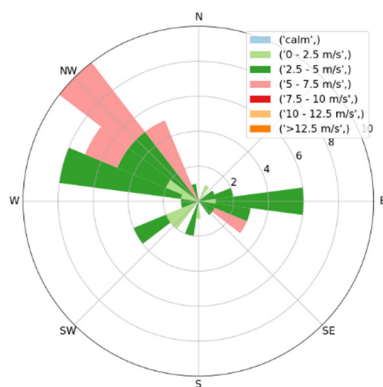
02.06–10.06



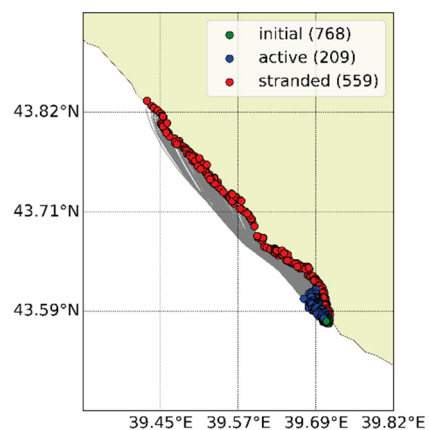
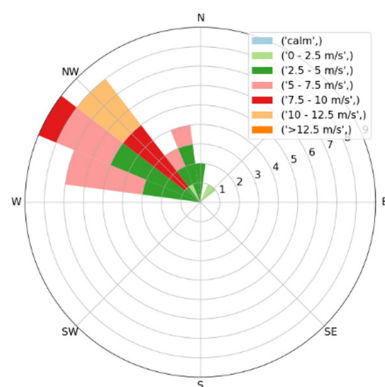
05.07–08.07



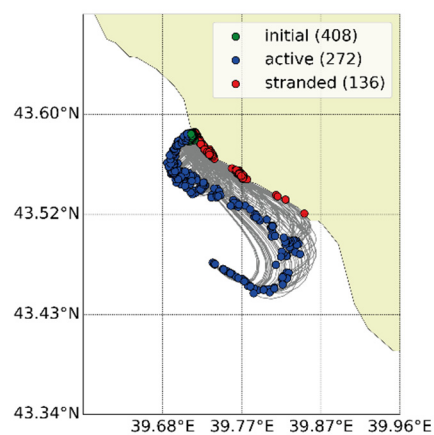
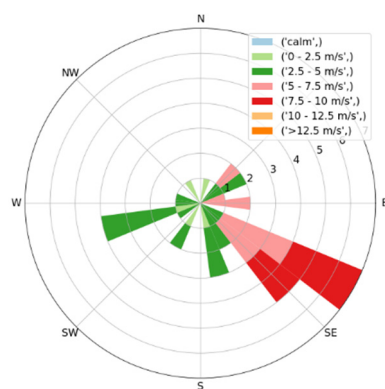
23.07–24.07



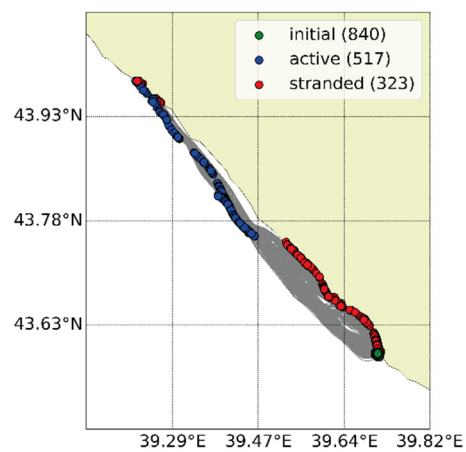
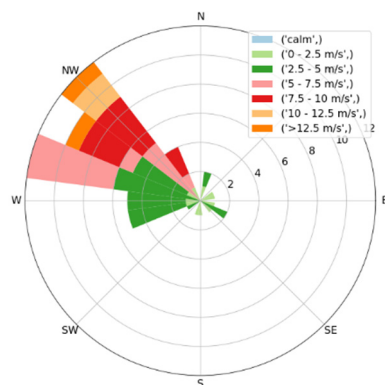
13.08



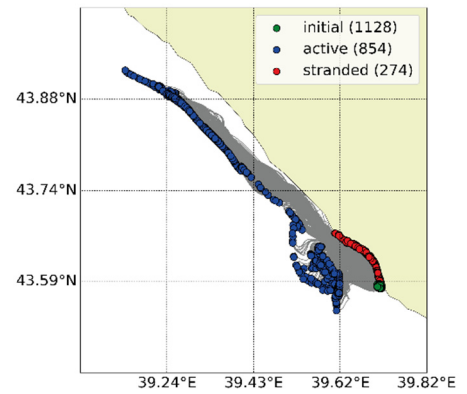
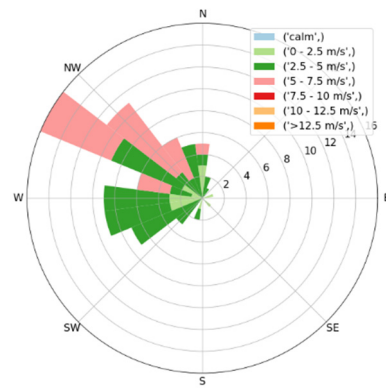
3.09



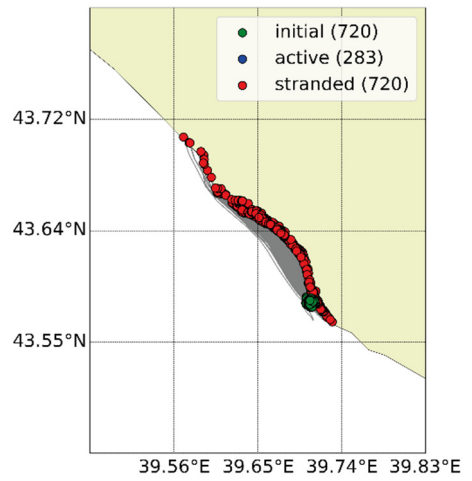
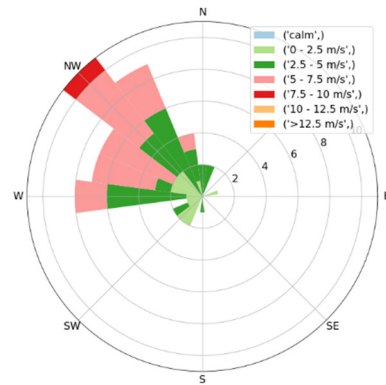
25.09–26.09



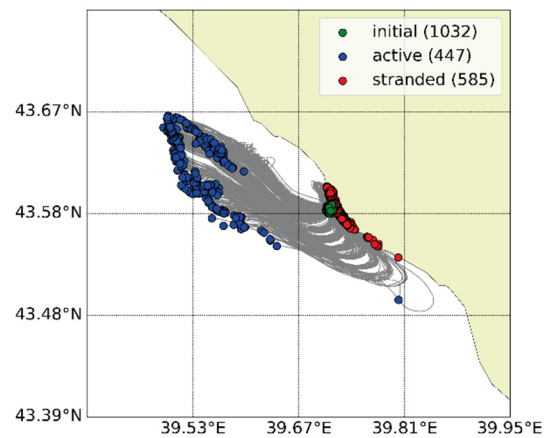
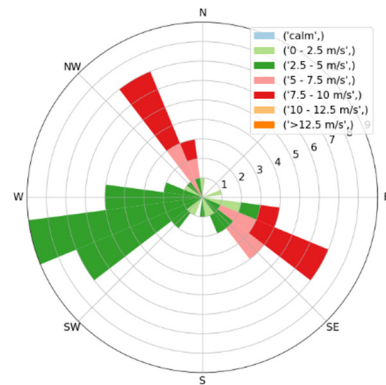
04.10–06.10



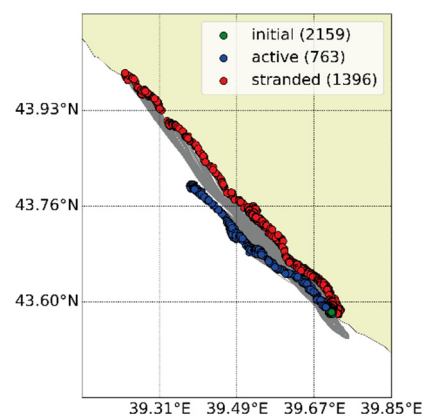
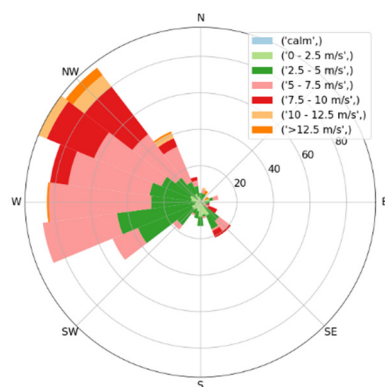
20.11–21.11



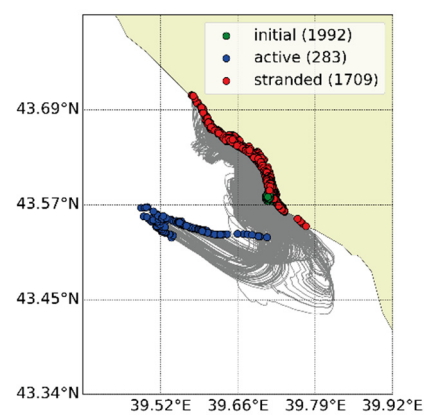
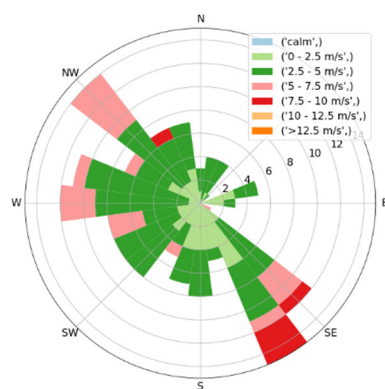
24.11–25.11



29.11–03.12



17.12–22.12



Supplementary Materials—2. Model of marine circulation INMOM

Numerical simulations of hydrophysical characteristics (i.e., current velocities and salinity, which were used in this study) were carried out using the Eulerian model of marine circulation INMOM (Institute of Numerical Mathematics Ocean Model).

S2.1. Governing Equations

The basic equations and numerical implementation are presented in detail in [1].

The INMOM is based on the primitive equations of ocean hydro- and thermodynamics written in generalized orthogonal coordinates on a sphere with a free surface boundary, assuming incompressible and hydrostatic fluid for the Boussinesq approximations. The vertical coordinate is a terrain-following, dimensionless σ -coordinate ($\sigma \in [0,1]$):

$$\sigma = \frac{z - \zeta}{H - \zeta}, \quad (S1)$$

where z is the standard vertical coordinate directed downward, H is the sea with an undisturbed surface, and ζ is the deviation of the sea surface height from the undisturbed state.

In accordance with [1], the model equations written in symmetrized form are:

$$D_t u - Z_\sigma (f + \eta) v = -\frac{Z_\sigma}{\rho_0 r_x} \left[\frac{\partial}{\partial x} \left(p - \frac{g}{2} Z_\rho \right) - \frac{g}{2} \left(\rho \frac{\partial Z}{\partial x} - Z \frac{\partial \rho}{\partial x} \right) \right] + \frac{1}{Z_\sigma} \frac{\partial}{\partial \sigma} K_U \frac{\partial u}{\partial \sigma} + D_u u, \quad (S2)$$

$$D_t v + Z_\sigma (f + \eta) u = -\frac{Z_\sigma}{\rho_0 r_y} \left[\frac{\partial}{\partial y} \left(p - \frac{g}{2} Z_\rho \right) - \frac{g}{2} \left(\rho \frac{\partial Z}{\partial y} - Z \frac{\partial \rho}{\partial y} \right) \right] + \frac{1}{Z_\sigma} \frac{\partial}{\partial \sigma} K_U \frac{\partial v}{\partial \sigma} + D_v v, \quad (S3)$$

$$\frac{\partial}{\partial \sigma} \left(p - \frac{g}{2} Z_\rho \right) = \frac{g}{2} \left(\rho \frac{\partial Z}{\partial \sigma} - Z \frac{\partial \rho}{\partial \sigma} \right), \quad (S4)$$

$$-\frac{\partial \zeta}{\partial t} + \frac{1}{r_x r_y} \left[\frac{\partial}{\partial x} (Z_\sigma r_y u) + \frac{\partial}{\partial y} (Z_\sigma r_x v) \right] + \frac{\partial \omega_\sigma}{\partial \sigma} = 0, \quad (S5)$$

$$D_t T = \frac{1}{Z_\sigma} \frac{\partial}{\partial \sigma} K_T \frac{\partial T}{\partial \sigma} + D_T T - \frac{\partial R}{\partial \sigma}, \quad (S6)$$

$$D_t S = \frac{1}{Z_\sigma} \frac{\partial}{\partial \sigma} K_S \frac{\partial S}{\partial \sigma} + D_S S, \quad (S7)$$

$$\rho = \rho(T, S, \hat{p}) \equiv \bar{\rho}(T + \bar{T}, S + \bar{S}, \hat{p}) - \bar{\rho}(\bar{T}, \bar{S}, \hat{p}). \quad (S8)$$

Here, x and y are generalized orthogonal coordinates in horizontal subspace; r_x and r_y are metric coefficients in spherical coordinates which compute as: $r_x = R_E \cos y$ and $r_y = R_E$, where R_E is the Earth's radius; vertical coordinate $Z = (H - \zeta)\sigma + \zeta$, $Z_\sigma = H - \zeta$, $Z_x \equiv \frac{\partial Z}{\partial x}$, $Z_y \equiv \frac{\partial Z}{\partial y}$.

The Coriolis parameter f is defined as $f = 2\tilde{\Omega} \sin \varphi$, where φ is geographical latitude and $\tilde{\Omega}$ is the Earth's angular velocity.

Parameter η is defined as:

$$\eta = \frac{1}{r_x r_y} \left(\frac{\partial r_y}{\partial x} v - \frac{\partial r_x}{\partial y} u \right) \quad (\text{S9})$$

The transport operator D_t is written in symmetrized form below:

$$\begin{aligned} D_t \psi \equiv D_t(\vec{u})\psi = & \frac{1}{2} \left(Z_\sigma \frac{\partial \psi}{\partial t} + \frac{\partial Z_\sigma \psi}{\partial t} \right) + \frac{1}{2 r_x r_y} \left[\frac{\partial}{\partial x} (Z_\sigma r_y u \psi) + Z_\sigma r_y u \frac{\partial \psi}{\partial x} \right. \\ & \left. + \frac{\partial}{\partial y} (Z_\sigma r_x v \psi) + Z_\sigma r_x v \frac{\partial \psi}{\partial y} \right] + \frac{1}{2} \left[\frac{\partial}{\partial \sigma} (\omega_\sigma \psi) + \omega_\sigma \frac{\partial \psi}{\partial \sigma} \right], \end{aligned} \quad (\text{S10})$$

where ψ is transported variable, $\vec{u} = (u, v, \omega_\sigma)$ is the velocity vector in the σ -coordinate system, and ω_σ is the vertical velocity in the σ -coordinate system defined as

$$\omega_\sigma = \omega - \left[(1 - \sigma) \frac{\partial \zeta}{\partial t} + \frac{u}{r_x} \frac{\partial Z}{\partial x} + \frac{v}{r_y} \frac{\partial Z}{\partial y} \right]. \quad (\text{S11})$$

T and S are deviations of potential temperature and salinity from their means \bar{T} and \bar{S} ; $\hat{p} = \rho_0 g Z$ is an approximate function of hydrostatic pressure; R is the penetrative solar radiation flux; ρ is the density computed according to [2]; ρ_0 is the reference density ($\rho_0 \approx 1$); K_U , K_T , and K_S are the coefficients of vertical turbulent viscosity and diffusivity.

The operators D_T and D_S describing lateral mixing of heat and salt along isopycnal surfaces are $D_T = D_S \equiv D_\psi$:

$$\begin{aligned} D_\psi \psi = & \frac{1}{r_x r_y} \frac{\partial}{\partial x} \left[\mu Z_\sigma \frac{r_y}{r_x} \left(\frac{\partial \psi}{\partial x} - \frac{\rho_x}{\rho_\sigma} \frac{\partial \psi}{\partial \sigma} \right) \right] - \frac{1}{r_x r_y} \frac{\partial}{\partial \sigma} \left[\mu Z_\sigma \frac{r_y}{r_x} \frac{\rho_x}{\rho_\sigma} \left(\frac{\partial \psi}{\partial x} - \frac{\rho_x}{\rho_\sigma} \frac{\partial \psi}{\partial \sigma} \right) \right] \\ & + \frac{1}{r_x r_y} \frac{\partial}{\partial y} \left[\mu Z_\sigma \frac{r_x}{r_y} \left(\frac{\partial \psi}{\partial y} - \frac{\rho_y}{\rho_\sigma} \frac{\partial \psi}{\partial \sigma} \right) \right] - \frac{1}{r_x r_y} \frac{\partial}{\partial \sigma} \left[\mu Z_\sigma \frac{r_x}{r_y} \frac{\rho_y}{\rho_\sigma} \left(\frac{\partial \psi}{\partial y} - \frac{\rho_y}{\rho_\sigma} \frac{\partial \psi}{\partial \sigma} \right) \right], \end{aligned} \quad (\text{S12})$$

where ψ is the diffused variable, μ is the lateral diffusion coefficient, $\rho_x \equiv \frac{\partial \rho_{pot}}{\partial x}$, $\rho_y \equiv \frac{\partial \rho_{pot}}{\partial y}$, and $\rho_\sigma \equiv \frac{\partial \rho_{pot}}{\partial \sigma}$. Turbulent viscosity operators D_u and D_v are a combination of laplacian and biharmonic operators in plain form that perform mixing along σ -surfaces [3].

Therefore, the INMOM is based on the complete primitive equations for horizontal velocities (S2)–(S4), hydrostatics, continuity (S5), heat and salt evolution (S6 and S7), and the equation of state (S8).

S2.2. Boundary conditions

At the sea's free surface ($\sigma = 0$) we applied the corresponding boundary conditions for momentum, heat and salt fluxes, turbulent kinetic energy, and dissipation frequency:

$$\begin{aligned} -\frac{K_U}{Z_\sigma} \frac{\partial u}{\partial \sigma} &= \frac{\tau_{ax}}{\rho_0}, -\frac{K_U}{Z_\sigma} \frac{\partial v}{\partial \sigma} = \frac{\tau_{ay}}{\rho_0}, \omega_\sigma = 0, \\ -\frac{K_T}{Z_\sigma} \frac{\partial T}{\partial \sigma} &+ \alpha_T (T - T_{obs}) = q_T, \\ -\frac{K_S}{Z_\sigma} \frac{\partial S}{\partial \sigma} &+ \alpha_S (S - S_{obs}) = q_S, \\ -\frac{K_U}{Z_\sigma \sigma_k} \frac{\partial k}{\partial \sigma} &= C_g (u_*^S)^3, -\frac{K_U}{Z_\sigma \sigma_\omega} \frac{\partial \omega}{\partial \sigma} = 0, \end{aligned} \quad (\text{S13})$$

where τ_{ax} and τ_{ay} are the wind stress components, α_T and α_S are the relaxation coefficients, q_T and q_S are the total heat and salt fluxes, C_g is the wind generation parameter [4–6], and

$$u_*^S = \left(\frac{\sqrt{\tau_{ax}^2 + \tau_{ay}^2}}{\rho_0} \right)^{1/2} \quad \text{is friction velocity in the upper ocean layer.}$$

Considering that there are no heat and salt fluxes as well as no flow across the bottom at the sea bottom ($\sigma = 1$), the following quadratic bottom friction conditions were prescribed:

$$\begin{aligned} \frac{K_U}{Z_\sigma} \frac{\partial u}{\partial \sigma} &= \frac{\tau_{bx}}{\rho_0}, \frac{K_U}{Z_\sigma} \frac{\partial v}{\partial \sigma} = \frac{\tau_{by}}{\rho_0}, \omega_\sigma = 0, \\ \frac{K_T}{Z_\sigma} \frac{\partial T}{\partial \sigma} &= 0, \frac{K_S}{Z_\sigma} \frac{\partial S}{\partial \sigma} = 0, \\ \frac{K_U}{Z_\sigma \sigma_k} \frac{\partial k}{\partial \sigma} &= C_g (u_*^B)^3, \frac{K_U}{Z_\sigma \sigma_\omega} \frac{\partial \omega}{\partial \sigma} = 0, \end{aligned} \quad (S14)$$

where $\tau_{bx} = -\rho_0 C_D \sqrt{u^2 + v^2 + e_b^2} u$ and $\tau_{by} = -\rho_0 C_D \sqrt{u^2 + v^2 + e_b^2} v$ are bottom stress components, drag coefficient $C_D = 2.5 \times 10^{-3}$, $e_b = 5$ cm/s are empirical constants, and

$$u_*^B = \left(\frac{\sqrt{\tau_{bx}^2 + \tau_{by}^2}}{\rho_0} \right)^{1/2} \quad \text{is friction velocity in the bottom ocean layer.}$$

At the lateral boundary normal velocity, normal derivatives of tangent velocity, heat, salt, turbulent kinetic energy, and dissipation frequency fluxes are assumed to be equal to zero.

The surface turbulent fluxes were calculated using bulk formulas [7].

We did not consider tidal forcing in the numerical simulation, as tidal currents in the Black Sea are low and do not significantly influence the general circulation of the sea [8].

Supplementary Materials—3. OpenDrift model

The presented particle drift simulations are based on the open-source, Python-based modeling framework OpenDrift developed by the Norwegian Meteorological Institute [9]. A subclass of OpenDrift is the Oceandrift model, which was used to simulate the transport of particles in the northeastern part of the Black Sea.

Each particle is moved due to the established surface current, wind, and Stokes drift velocities at its new location, which is described by longitude and latitude. For our study simulations, we used current velocity fields from the INMOM model run with a 1-hr temporal resolution, wind fields from the WRF model, and Stokes drift velocity fields taken from the reanalysis data of the European CMEMS service (<https://data.marine.copernicus.eu/products>).

The position of particle $\mathbf{x}(t) = (x(t), y(t))$ is defined by the integration of the equations system [10]:

$$\begin{cases} \frac{d\mathbf{x}(t)}{dt} = \mathbf{u}_c(\mathbf{x}(t), t) + \mathbf{u}_w(\mathbf{x}(t), t) + \mathbf{u}_s(\mathbf{x}(t), t) \\ \mathbf{x}(t_0) = \mathbf{x}_0 \end{cases}$$

where \mathbf{x}_0 is the initial element position at time t_0 , $\mathbf{u}_s(\mathbf{x}(t), t)$ is Stokes drift velocity, $\mathbf{u}_c(\mathbf{x}(t), t)$ is current velocity, and $\mathbf{u}_w(\mathbf{x}(t), t)$ is wind drag velocity.

Wind drag velocity is defined as:

$$\mathbf{u}_w(\mathbf{x}(t), t) = 0.02 \mathbf{U}_{10}(\mathbf{x}(t), t),$$

where $\mathbf{U}_{10}(\mathbf{x}(t), t)$ is the wind velocity at 10 m.

The advection scheme is a Euler-forward scheme, and the time step for the particles simulations is 60 min. At every time step, current, wind, and Stokes drift velocities are interpolated to the corresponding particles' locations.

No additional diffusion displacement was added to the advection of particles, as we wanted to investigate the effects of external forces without adding any random "disturbances" to the motion equation. In order to investigate the

main flow directions, a number of floating Lagrangian particles, proportional to the rivers' discharges, were released every hour in grid cells of 250 m × 250 m in the vicinity of the small river mouths.

References

1. Moshonkin, S.; Zalesny, V.; Gusev, A. Simulation of the Arctic-North Atlantic Ocean Circulation with a Two-Equation k-omega Turbulence Parameterization. *J. Mar. Sci. Eng.* **2018**, *6*, 95. <https://doi.org/10.3390/jmse6030095>.
2. Brydon, D.; Sun, S.; Bleck, R. A new approximation of the equation of state for seawater, suitable for numerical ocean models. *J. Geophys. Res. Oceans*, **1999**, *104*, 1537–1540. <https://doi.org/10.1029/1998JC900059>.
3. Zalesny, V.; Marchuk, G.; Agoshkov, V.; Bagno, A.; Gusev, A.; Diansky, N.; Moshonkin, S.; Tamsalu, R.; Volodin, E. Numerical simulation of large-scale ocean circulation based on the multicomponent splitting method. *Russ. J. Numer. Anal. Math. Model.* **2010**, *25*, 581–609. <https://doi.org/10.1515/rjnamm.2010.036>.
4. Noh, Y.; Ok, H.; Lee, E.; Toyoda, T.; Hirose, N. Parameterization of Langmuir Circulation in the Ocean MixedLayer Model Using LES and Its Application to the OGCM. *J. Phys. Oceanogr.* **2016**, *46*, 57–78. <https://doi.org/10.1175/JPO-D-14-0137.1>.
5. Miropolski, Y.Z. Non-stationary model of the layer of the convective-wind mixing in the ocean. *Izv. Atmos. Ocean. Phys.* **1970**, *6*, 1284–1294.
6. Zaslavskii, M.; Zalesny, V.; Kabatchenko, I.; Tamsalu, R. On the self-adjusted description of the atmospheric boundary layer, wind waves, and sea currents. *Oceanology* **2006**, *46*, 159–169. <https://doi.org/10.1134/S0001437006020020>
7. Gill, A. *Atmosphere-Ocean Dynamics*; Academic Press: New York, 1982; 662p.
8. Osadchiev, A.A.; Korshenko, E.A. Small River Plumes off the Northeastern Coast of the Black Sea under Average Climatic and Flooding Discharge Conditions. *Ocean Sci.* **2017**, *13*, 465–482. <https://doi.org/10.5194/os-13-465-2017>.
9. Dagestad, K.-F.; Röhrs, J.; Breivik, Ø.; Ådlandsvik, B. OpenDrift v1.0: A Generic Framework for Trajectory Modelling. *Geosci. Model Dev.* **2018**, *11*, 1405–1420. <https://doi.org/10.5194/gmd-11-1405-2018>.
10. Bruciaferri, D.; Tonani, M.; Lewis, H.W.; Siddorn, J.R.; Saulter, A.; Castillo Sanchez, J.M.; Valiente, N.G.; Conley, D.; Sykes, P.; Ascione, I.; McConnell, N. The impact of ocean-wave coupling on the upper ocean circulation during storm events. *J. Geophys. Res. : Ocean.* **2021**, *126*, e2021JC017343. <https://doi.org/10.1029/2021JC017343>.